Concomitant systolic and diastolic alterations during chronic hypertension in pig

Mathieu Jozwiak, Albano C Meli, Jonathan Melka, Mario Rienzo, Alexandra d'Anglemont de Tassigny, Nathalie Saint, Alain Bize, Lucien Sambin, Valérie Scheuermann, Olivier Cazorla, et al.

▶ **To cite this version:**

Mathieu Jozwiak, Albano C Meli, Jonathan Melka, Mario Rienzo, Alexandra d'Anglemont de Tassigny, et al.. Concomitant systolic and diastolic alterations during chronic hypertension in pig. Journal of Molecular and Cellular Cardiology, 2019, 131, pp.155-163. 10.1016/j.yjmcc.2019.04.027 . hal-02120090

HAL Id: hal-02120090
https://hal.science/hal-02120090

Submitted on 5 Jun 2020

HAL is a multi-disciplinary open access archive for the deposit and dissemination of scientific research documents, whether they are published or not. The documents may come from teaching and research institutions in France or abroad, or from public or private research centers.

L'archive ouverte pluridisciplinaire **HAL**, est destinée au dépôt et à la diffusion de documents scientifiques de niveau recherche, publiés ou non, émanant des établissements d'enseignement et de recherche français ou étrangers, des laboratoires publics ou privés.

Concomitant systolic and diastolic alterations during chronic hypertension in pig

Mathieu Jozwiak[a], Albano C. Meli[b,1], Jonathan Melka[a,1], Mario Rienzo[a], Alexandra d'Anglemont de Tassigny[a], Nathalie Saint[b], Alain Bizé[a], Lucien Sambin[a], Valérie Scheuermann[b], Olivier Cazorla[b], Luc Hittinger[a], Alain Berdeaux[a], Jin-Bo Su[a], Belaid Bouhemad[c], Alain Lacampagne[b,*], Bijan Ghaleh[a,**]

[a] *U955-IMRB, Equipe 03, Inserm, UPEC, Ecole Nationale Vétérinaire d'Alfort, Maisons-Alfort, France*
[b] *PhyMedExp, University of Montpellier, INSERM, CNRS, CHRU Montpellier, Montpellier, France*
[c] *Service d'Anesthésie-Réanimation Chirurgicale, CHU de Dijon, 14 rue Paul Gaffarel, 21079 Dijon, France*

Keywords:
Contractile function
Left ventricular hypertrophy
Calcium handling
Ryanodine receptor

A B S T R A C T

The mechanical and cellular relationships between systole and diastole during left ventricular (LV) dysfunction remain to be established. LV contraction-relaxation coupling was examined during LV hypertrophy induced by chronic hypertension. Chronically instrumented pigs received angiotensin II infusion for4weeks to induce chronic hypertension (133 ± 7 mmHg *vs* 98 ± 5 mmHg for mean arterial pressure at Day 28 *vs* 0, respectively) and LV hypertrophy. LV function was investigated with the instrumentation and echocardiography for LV twist-untwist assessment before and after dobutamine infusion. The cellular mechanisms were investigated by exploring the intracellular Ca^{2+} handling. At Day 28, pigs exhibited LV hypertrophy with LV diastolic dysfunction (impaired LV isovolumic relaxation, increased LV end-diastolic pressure, decreased and delayed LV untwisting rate) and LV systolic dysfunction (impaired LV isovolumic contraction and twist) although LV ejection fraction was preserved. Isolated cardiomyocytes exhibited altered shortening and lengthening. Interestingly, contraction-relaxation coupling remained preserved both *in vivo* and *in vitro* during LV hypertrophy. LV systolic and diastolic dysfunctions were associated to post-translational remodeling and dysfunction of the type 2 cardiac ryanodine receptor/Ca^{2+} release channel (RyR2), *i.e.*, PKA hyperphosphorylation of RyR2, depletion of calstabin 2 (FKBP12.6), RyR2 leak and hypersensitivity of RyR2 to cytosolic Ca^{2+} during both contraction and relaxation phases. In conclusion, LV contraction-relaxation coupling remained preserved during chronic hypertension despite LV systolic and diastolic dysfunctions. This implies that LV diastolic dysfunction is accompanied by LV systolic dysfunction. At the cellular level, this is linked to sarcoplasmic reticulum Ca^{2+} leak through PKA-mediated RyR2 hyperphosphorylation and depletion of its stabilizing partner.

1. Introduction

Left ventricular contraction-relaxation coupling has been previously investigated in healthy subjects [4,7] or in patients with myocardial ischemia [10] but not during chronic hypertension and LV hypertrophy. This coupling implies concomitant adaptations but also alterations of diastole and systole. In this context, investigation of LV twist and untwist that result from the helical LV myocardial fiber architecture, is an interesting approach [2]. More precisely, the systolic LV wringing motion or LV twist occurs during isovolumic contraction and during the ejection period [2]. LV untwist occurs mainly during isovolumic relaxation before filling and is an important determinant of the early diastolic LV filling [4]. LV twist allows sarcomeres to store potential energy and create restoring forces [20], which are released during LV untwist and contribute to the diastolic suction [20]. Previous studies have shown that in patients with systemic hypertension, LV twist could be preserved [18,27] or increased [1,5] but decreased when LV ejection fraction was impaired [14]. However, LV untwist was always decreased whatever the LV ejection fraction [5,15,18,27].

Accordingly, in the present study, we investigated changes in LV

* Corresponding author at: INSERM U1046, CHU Arnaud de Villeneuve, 371 avenue du Doyen G. Giraud, 34295 Montpellier, Cedex 05, France.
** Corresponding author at: INSERM U955 Equipe 03, Faculté de Médecine, 8 rue du Général Sarrail, 94000 Créteil, France.
E-mail addresses: alain.lacampagne@inserm.fr (A. Lacampagne), bijan.ghaleh@inserm.fr (B. Ghaleh).
[1] Authors equally contributed.

twist-untwist relationship to apprehend the contraction-relaxation coupling in a pig model of chronic hypertension and LV hypertrophy induced by angiotensin II infusion [24,25]. In addition, we also investigated potential underlying cellular and molecular mechanisms by focusing on the intracellular calcium handling machinery knowing that intracellular calcium and its handling affect cardiac contraction and relaxation.

2. Methods

The experiments were in agreement with the local animal ethical committee [ComEth AFSSA-ENVA-UPEC agreement #11-0059].

2.1. Experimental design

Hypertension was induced in nine chronically instrumented pigs (Land race White crossed, Lebeau, Gamblais France, 3 ± 1 months, 28 ± 1 and 34 ± 1 kg at Days 0 and 28 of the protocol, respectively) by four weeks of continuous angiotensin II infusion at 30 ng/kg/min using an external portable peristaltic pump [24,25]. At Day 0 (before starting angiotensin II infusion), hemodynamic and echocardiographic measurements were performed in basal condition and during increased chronotropic and inotropic stress states induced by dobutamine infusion (10 µg/kg/min). At Day 28, similar measurements were performed 1 h after stopping the angiotensin II infusion to minimize the impact of changes in loading conditions, *i.e.*, to evaluate the intrinsic LV contractile properties. Due to ethical considerations in order to reduce as much as possible the number of investigated animals, eight pigs were derived from a previous study [12]. Furthermore, each animal served as it own control. Using the same experimental setting, we previously compared saline and angiotensin II-infused pigs [24,25] and clearly showed that the development of LV dysfunction and hypertrophy are true and not related to pig growth. For *in vitro* analyses, we used a control group. Cardiomyocytes were also freshly isolated for functional investigations and cardiac ventricle samples were rapidly taken from both angiotensin II- and saline-infused animals and frozen in liquid nitrogen for biochemical experiments exploring RyR2.

2.2. Hemodynamic measurements

All hemodynamic data were recorded (1 kHz), digitized and analyzed using HEM v4.2 software (Notocord Systems, Croissy sur Seine, France). Aortic and left atrial pressures, LV end-diastolic pressure and the time constant of isovolumic LV pressure decay (Tau) were measured and calculated as previously described [24].

2.3. Echocardiographic data acquisition analysis

Echocardiographic examinations were performed using a Vivid 7 echocardiograph (GE Healthcare, Horten, Norway) with a 3.5-MHz transducer at high frame rates (range 68–80 frame/s). For all measurements, three consecutive cardiac cycles were stored digitally for blinded offline analysis (EchoPac 6.0, GE Healthcare). The LV mass was estimated from LV linear dimensions and LV ejection fraction was calculated by the biplane Simpson method [14]. From the apical four chamber view, mitral inflow (E and A waves) at pulsed Doppler was obtained. The LV systolic (S) and early diastolic (e') peak velocities of the lateral and septal mitral annulus at tissue Doppler imaging were also measured and averaged (LV $S_{averaged}$ and LV $e'_{averaged}$). Isovolumic contraction and relaxation times were derived by placing the pulsed Doppler gate in the LV outflow tract near the mitral valves to simultaneously record LV outflow signal and mitral inflow [19]. The timing of valve closure and opening was measured from the LV outflow signal and mitral inflow at pulsed Doppler. The start of the systole was set 10 milliseconds before the peak of the R wave.

2.4. Speckle tracking analysis

LV twist was calculated as the instantaneous difference between the maximum LV apical and basal rotations and was expressed in degrees [2]. The LV untwisting rate, which represents the maximum velocity of the diastolic myocardial LV deformation, was calculated and expressed in degrees.s^{-1}. LV twisting and untwisting rates were calculated as the first derivative over time of the LV twist waveform. Here, the LV twisting rate represents the maximum velocity of the systolic myocardial LV deformation and the LV untwisting rate represents the maximum velocity of the diastolic myocardial LV deformation. The extent of untwist during the isovolumic relaxation time (UT_{IVRT}), expressed as percentage of LV twist, was calculated as follow: $UT_{IVRT} = 100 \times (twist - twist_{MVO})/twist$, where $twist_{MVO}$ was the LV twist at the mitral valve opening [12].

2.5. Cardiomyocyte contractility and intracellular calcium transient

The myocardium was perfused through the left anterior descending coronary artery (~1–2 ml/min, 37 °C, 30 min) with Ca^{2+}-free Tyrode's solution (in mM: NaCl 130, KCl 5.4, KH_2PO_4 1.2, $MgSO_4$ 1.2, Na–Hepes 6.0, glucose 10 (pH = 7.20) followed by the same calcium-free perfusion buffer supplemented with 1.4 mg/ml collagenase A (Boehringer Mannheim) and 0.1 mg/ml protease (type XIV, Sigma) and finally a low Ca^{2+} Tyrode's solution. Tissues were sliced and cellular dissociation was achieved by gentle mechanical agitation. These preparations were minced, filtered through a nylon mesh and the cells resuspended in low Ca^{2+} Tyrode's solution. After 20 min, extracellular calcium was added incrementally up to 1.8 mM $CaCl_2$. Ca^{2+}-tolerant cells were stored at room temperature and used within 8–10 h after isolation.

Myocytes were then transferred to a continuously perfused cell chamber placed on an inverted microscope (in mM, NaCl 140, KCl 5.4, $CaCl_2$ 1, $MgCl_2$ 0.8, HEPES 10 and glucose 5.6; pH = 7.4, 37 °C). Myocytes were paced at 1 Hz and cell images were continuously acquired by a 240 samples/s charge coupled device video camera through a x 40 objective lens. Sarcomere shortening was measured as percent sarcomere shortening, *i.e.*, defined as the difference between the systolic and the diastolic sarcomere lengths divided by the diastolic sarcomere length. The maximal rate of shortening and lengthening were also calculated.

Calcium transient were also assessed using the ratiometric fluorescent Ca^{2+} indicator fura-2 (Invitrogen, Illkirch, France). Fura-loaded myocytes (5 µM) were excited at 340 nm and 380 nm, and the resulting fluorescence was measured at 510 nm. The fluorescence ratio was obtained by dividing the calculated 340 nm by excited fluorescence by the measured 380 nm excited fluorescence (340/380 nm). The amplitude of intracellular Ca^{2+} changes was measured as the difference between baseline and peak fluorescence ratios using IonWizard data acquisition system (Ionoptix).

2.6. Sarcoplasmic reticulum vesicle preparation

200 to 500 mg of LV myocardial tissue from pigs treated with saline or angiotensin II were homogenized using a tissue homogenizer (Fisher Scientific) at the highest speed for 1 min with 1 to 2 ml of 300 mM sucrose, 20 mM imidazole (pH = 7.4) and EDTA-free protease inhibitors (Roche). Homogenate was centrifuged at 8000 *g* for 20 min at 4 °C. While the supernatant was stored on ice, the pellet was homogenized for a second run using a tissue homogenizer and centrifuged in similar conditions as above. The first and second supernatants were pooled and centrifuged at 40,000 *g* for 60 min at 4 °C. While the supernatant was discarded, the final pellet containing SR fractions was resuspended in 100 to 200 µl and aliquoted using the same buffer as above. Samples were frozen in liquid nitrogen and stored at −80 °C.

2.7. Planar lipid bilayer measurements

SR vesicles containing RyR2 were fused to planar lipid bilayers formed by painting a lipid solution of azolectin (type IV S from Sigma) at 45 mg/ml in decane as previously published [6,17]. The channel properties including Po, To, Tc and Fo were determined as previously published [17].

2.8. RyR2 co-immunoprecipitation and Western blotting

Left ventricular samples were lysed in 1 ml of a buffer containing Tris maleate 10 mM (pH = 6.8), NaF 35 mM, triton 1% and protease inhibitors (Roche 11,873,580,001). An anti-RyR antibody was used to immunoprecipitate RyR2 from 500 µg of LV homogenate. The samples were incubated with anti-RyR antibody in 0.5 ml of a modified RIPA buffer (TrisHCl 10 mM (pH = 7,4), NaCl 150 mM, Triton 1%, NaF 5 mM and protease inhibitor cocktail) for 2 h at 4 °C. The immune complexes were incubated with protein A/G magnetic beads (Pierce 88,802) at 4 °C for 2 h, after which the beads were washed three times with RIPA buffer.

To detect RyR2 protein oxidation, the immune complexes were treated with 2,4 dinitrophenylhydrazine (DNPH) and the DNP-derivatized carbonyls were detected using an Oxyblot Protein oxidation detection Kit (Millipore S7150).

Proteins were separated on SDS/PAGE gels and transferred onto nitrocellulose membranes for 1 h at 100 Volts. The immunoblots were prepared using antibodies against RyR (1:1000), phospho-epitope–-specific antibody to human RyR1 phosphorylated at Ser-2808 (1:5000), which detects mouse PKA-phosphorylated RyR1 (at Ser-2844) and RyR2 (at Ser-2808), anti Cys-NO antibody (Sigma-Aldrich N5411, 1:1000), anti-DNPH(1:300) and anti FKBP 12.6 (RD System AF 4174, 1:1000). To quantify the expression of SERCA2a and phospholamban (PLB), immunoblots were prepared using antibodies against SERCA2a (Badrilla A010–20, 1:1000), PLB (Abcam ab85146, 1:1000), anti phospho-PLB at Ser16 (Badrilla A010–12, 1:1000) and GAPDH (Abcamab 8245, 1:60000). All immunoblots were developed and quantified using the Odyssey infrared imaging system (LICOR Biosystems) and infrared-labeled secondary antibodies.

2.9. Statistical analysis

Variables are expressed as mean ± SEM. Statistical analysis was performed using Prism (v6.0, GraphPad). Comparisons between the two samples were performed by two-sided paired Student's *t*-test or independent Student's *t*-test. Correlations between variables were analyzed using linear regression and tested by Pearson's coefficient correlation. Statistical significance was fixed at $p < .05$.

3. Results

3.1. Development of LV hypertrophy and LV dysfunction

Chronic infusion of angiotensin II induced a significant increase in mean arterial pressure and maximal LV pressure (133 ± 7 *vs* 98 ± 5 mmHg and 156 ± 10 *vs*115 ± 7 mmHg at Day 28 *vs* Day 0, respectively). In order to analyze LV characteristics and performance independently from changes in loading conditions as a result of hypertension, all measurements were performed 1 h after stopping the infusion of angiotensin II (Table 1). In these conditions, we could observe increases in LV posterior wall thickness (12.0 ± 0.2 mm at Day 28 *vs.* 5.7 ± 0.2 mm at Day 0), septal wall thickness (11.8 ± 0.2 mm at Day 28 *vs.* 5.4 ± 0.2 mm at Day 0) and estimated LV mass (236 ± 9 g at Day 28 *vs.* 71 ± 5 g at Day 0), indicating LV hypertrophy, in accordance with our previous studies using the same experimental design and comparing Angiotensin II- to saline-infused pigs [23,24]. This was confirmed by LV weight measured at Day 28 during sacrifice (LV weight: 232 ± 18 g). Left atrium was significantly enlarged (18.9 ± 1.1 mm at Day 28 *vs.* 11.3 ± 0.3 mm at Day 0). At Day 28, heart rate was significantly increased as compared to Day 0 (105 ± 5 *vs.* 77 ± 3 beats/min, respectively) (Table 1).

Table 1
Hemodynamic and echocardiographic parameters at Day 0 and Day 28 (recordings performed 1 h after stopping the angiotensin-II infusion).

Parameter	Day 0	Day 28
Hemodynamic parameters		
Heart rate (beats/min)	77 ± 3	93 ± 8*
Mean arterial pressure (mmHg)	98 ± 5	105 ± 5
Echocardiographic diastolic parameters		
Transmitral E/A ratio	1.28 ± 0.03	1.42 ± 0.03*
LV $e'_{averaged}$ ($cm.s^{-1}$)	9.6 ± 0.5	6.8 ± 0.4*
LV $E/e'_{averaged}$ ratio	6.3 ± 0.4	10.7 ± 0.7*
Isovolumic relaxation time (ms)	70 ± 2	74 ± 2*
LV untwisting velocity at MVO ($°.s^{-1}$)	−138 ± 10	−71 ± 9*
UT_{IVRT} (% of twist)	24 ± 3	7 ± 1*
Echocardiographic systolic parameters		
LV ejection fraction (%)	61 ± 2	62 ± 2
Isovolumic contraction time (ms)	50 ± 2	56 ± 2*
LV $S_{averaged}$ ($cm.s^{-1}$)	6.7 ± 0.4	5.4 ± 0.2*

Data are expressed as mean ± SEM.
LV: left ventricular; MVO: mitral valve opening; $UT_{IVRT:}$ extent of untwist during the isovolumic relaxation time.
* $p < .05$ Day 0 *vs.* Day 28, n = 9.

As shown in Table 1 and Fig. 1B-D, these hypertrophied hearts were characterized by LV diastolic dysfunction as assessed by the increase in Tau (+22%) and LV end-diastolic pressure (+63%) as well as decreases in LV untwisting rate (−30%) and LV untwist-related parameters. Other echocardiographic parameters showing LV diastolic dysfunction are also summarized in Table 1. As illustrated in Fig. 1A, LV untwisting rate was also delayed in the cardiac cycle at Day 28, occurring 48 ± 12 ms after the mitral valve opening as opposed to 10 ± 4 ms before the mitral valve opening at Day 0 (Fig. 1A). There was a significant correlation between the delay in LV untwisting rate and the increase in LV end-diastolic pressure ($r = 0.74$, $p < .0001$).

At Day 28, we observed concomitant systolic dysfunction despite preserved LV ejection fraction. As shown in Table 1 and Fig. 1E–G, there was a significant decrease in LV twist (−32%), resulting from decreases in LV apical (−16%) and basal (−40%) rotations. Paradoxically, along with a significant increase in heart rate, isovolumic contraction time was slightly but significantly increased. Other echocardiographic parameters indicating LV systolic dysfunction are also summarized in Table 1.

3.2. Contraction-relaxation coupling during chronic hypertension and LV hypertrophy

To evaluate the contraction-relaxation coupling, we next analyzed the relationships between LV twist and LV untwisting rate and observed a strong correlation (Fig. 2A). Similarly, LV twist and isovolumic relaxation time (Fig. 2B) as well as LV untwisting rate and isovolumic contraction time (Fig. 2C) were significantly correlated. Importantly, the ratio between LV twist and untwisting rate remained unchanged between Day 0 and Day 28 (0.109 ± 0.011 *vs.* 0.107 ± 0.011, respectively). Therefore, the coupling between myocardial contraction and relaxation remained preserved despite LV systolic and diastolic dysfunctions in our model of chronic hypertension and LV hypertrophy. Importantly, there was a strong and significant negative relationship between LV end-diastolic pressure and LV twist (Fig. 2D), which clearly associates the alteration of LV twist with LV diastolic dysfunction. Similarly, LV end-diastolic pressure was also strongly and significantly correlated with LV untwisting rate (Fig. 2E). All these results highlight the concomitant alterations in LV twist and untwist. Hence, LV diastolic alterations are concomitant to LV systolic alterations although LV

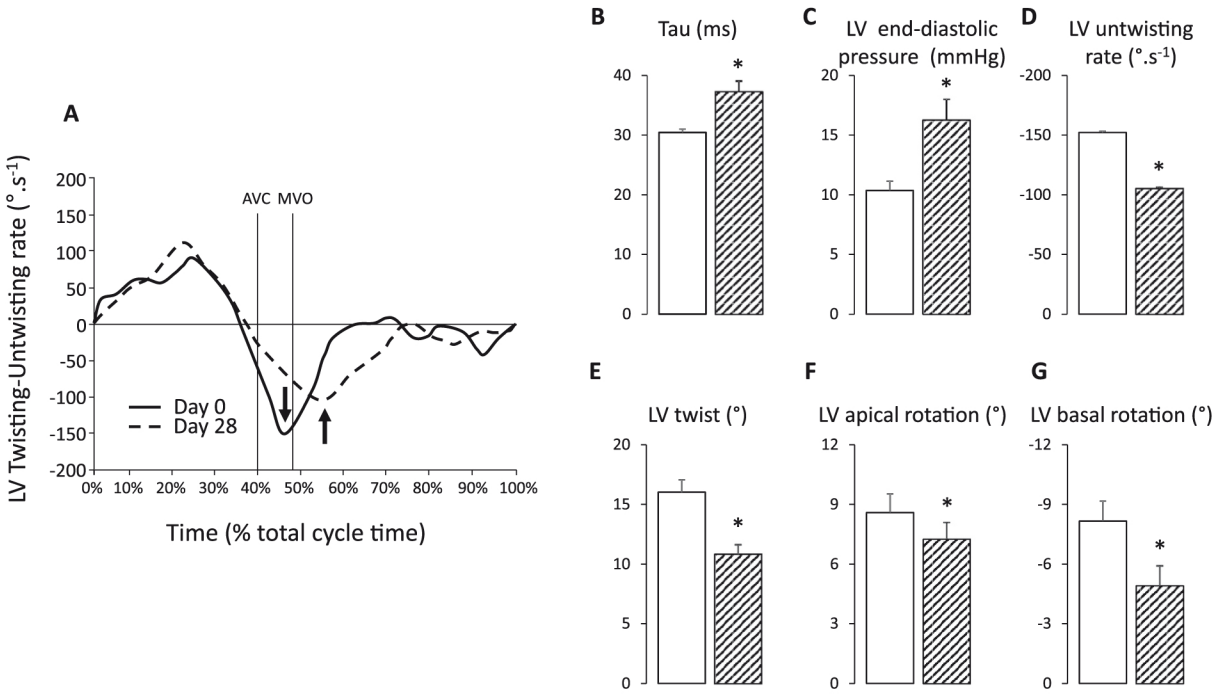

Fig. 1. Left ventricular systolic and diastolic dysfunctions. Representative waveforms of LV twisting and untwisting rate (A) during one cardiac cycle obtained at Day 0 and after four weeks of angiotensin II infusion (Day 28). The onset and the end of cardiac cycle represent 0% and 100% of the total cycle time (n = 9), respectively (AVC = aortic valve closure, MVO = mitral valve opening). Arrows indicate the maximum velocity of the LV diastolic deformation and show that at Day 28, this particular point of the cycle occurred later un the cardiac cycle as compared to Day 0, in particular after the mitral valve opening. Diastolic function: mean ± SEM values of time constant of left ventricular (LV) isovolumic pressure decay Tau (B), LV end-diastolic pressure (C) and LV untwisting rate (D). Systolic function: mean ± SEM values of LV twist (E) and its components LV apical (F) and basal (G) rotations. All these parameters were evaluated at Day 0 (open bars) and at Day 28 after four weeks of angiotensin II infusion (hatched bars). n = 7 for Tau and n = 9 for echocardiographic parameters *p < .05 *vs.* Day 0.

ejection fraction is preserved.

3.3. Aberrant cardiac intracellular calcium handling upon chronic hypertension and LV hypertrophy

We further investigated isolated cardiomyocytes function. Both cardiomyocyte shortening and rate of shortening were significantly reduced in angiotensin II- *vs.* saline-treated animals (Fig. 3A and B). The rate of lengthening was also significantly reduced (Fig. 3C). The ratio of shortening over lengthening rate remained similar between the two groups (−1.24 ± 0.21 *vs.* −1.62 ± 0.27 in angiotensin II- *vs.* saline-treated animals, respectively, p = NS), indicating a preserved cellular contraction-relaxation coupling. The Ca^{2+} transient amplitude was reduced in angiotensin II-treated animals (Fig. 3D to F) without significant changes in baseline diastolic Ca^{2+} and in the decay phase.

Aberrant intracellular Ca^{2+} handling is associated with systolic and diastolic dysfunctions. In particular, RyR2, the main intracellular Ca^{2+} release channels during contraction, have been reported to exhibit impairment responsible for aberrant SR Ca^{2+} leak in several cardiac disorders [8,11,26,29]. Thus, we investigated the RyR2-channel activity by isolating the SR microsomes from cardiac tissues and using the planar lipid bilayer technique (Fig. 4A–B). At low Ca^{2+} concentration (150 nmol/L, corresponding to the cytosolic [Ca^{2+}] during relaxation), angiotensin II-treated pigs showed a significant higher open probability (mean Po of 0.152 ± 0.056) as compared to saline-treated animals (mean Po of 0.008 ± 0.003, Fig. 4C), suggesting that RyR2 in angiotensin II-treated animals were leaky during relaxation. Interestingly, at systolic Ca^{2+} concentration (700 nmol/L), there was also a significant higher Po of the RyR2 channels in angiotensin II-treated animals. In addition, the RyR2 in angiotensin II-treated animals exhibited higher sensitivity to cytosolic Ca^{2+} as indicated by higher Po for each Ca^{2+} concentration compared to saline-treated animals [(EC_{50}:275*vs.* 629 nmol/L, respectively, and the left shift of the Ca^{2+} dose-response (Fig. 4D)]. Overall, these results demonstrated that RyR2 channels exhibit an aberrant Ca^{2+} release during both contraction and relaxation in angiotensin II-treated animals.

We and others have shown that leaky RyR2 result from post-translational modifications of the RyR2 macromolecular complex [9,17,26]. As shown in Fig. 4E–F, the ratio of PKA-phosphorylated RyR2 at Ser-2808 to total RyR2 were markedly increased in angiotensin II-treated animals, indicating RyR2 hyperphosphorylation at its specific site of Ser-2808 while oxidation and S-nitrosylation levels remained unchanged (Fig. 4H). Importantly, the ratio of calstabin2 (FKBP12.6), which stabilizes the closed conformation of RyR2, to total RyR2 was concomitantly and markedly reduced in angiotensin II treated animals, indicating a reduced association of calstabin2 to RyR2 (Fig. 4E and I). These data suggest that the angiotensin II treatment causes PKA hyperphosphorylation of RyR2 and calstabin2 depletion from the RyR2 macromolecular. In addition, this was accompanied by reduced SERCA2a and PLB but increased phospho-PLB expression in the angiotensin II-treated animals (Fig. 5A-D).

4. Discussion

In the present study, chronic hypertension and LV hypertrophy induced by the infusion of angiotensin II in pigs elicited LV diastolic dysfunction that was accompanied by LV systolic dysfunction while LV ejection fraction was preserved. At the cellular level, we observed a remodeling of RyR2 that were leaky and hypersensitive to cytosolic Ca^{2+} during both contraction and relaxation phases. These alterations were associated with post-translational modifications of RyR2 with PKA-hyperphosphorylation and depletion of its stabilizing protein calstabin2 (FKBP12.6). Despite this aberrant intracellular calcium handling, the contraction-relaxation coupling remained preserved, *i.e.*, the occurrence of LV diastolic dysfunction was accompanied with LV systolic dysfunction. *In vivo* functional parameters were obtained in

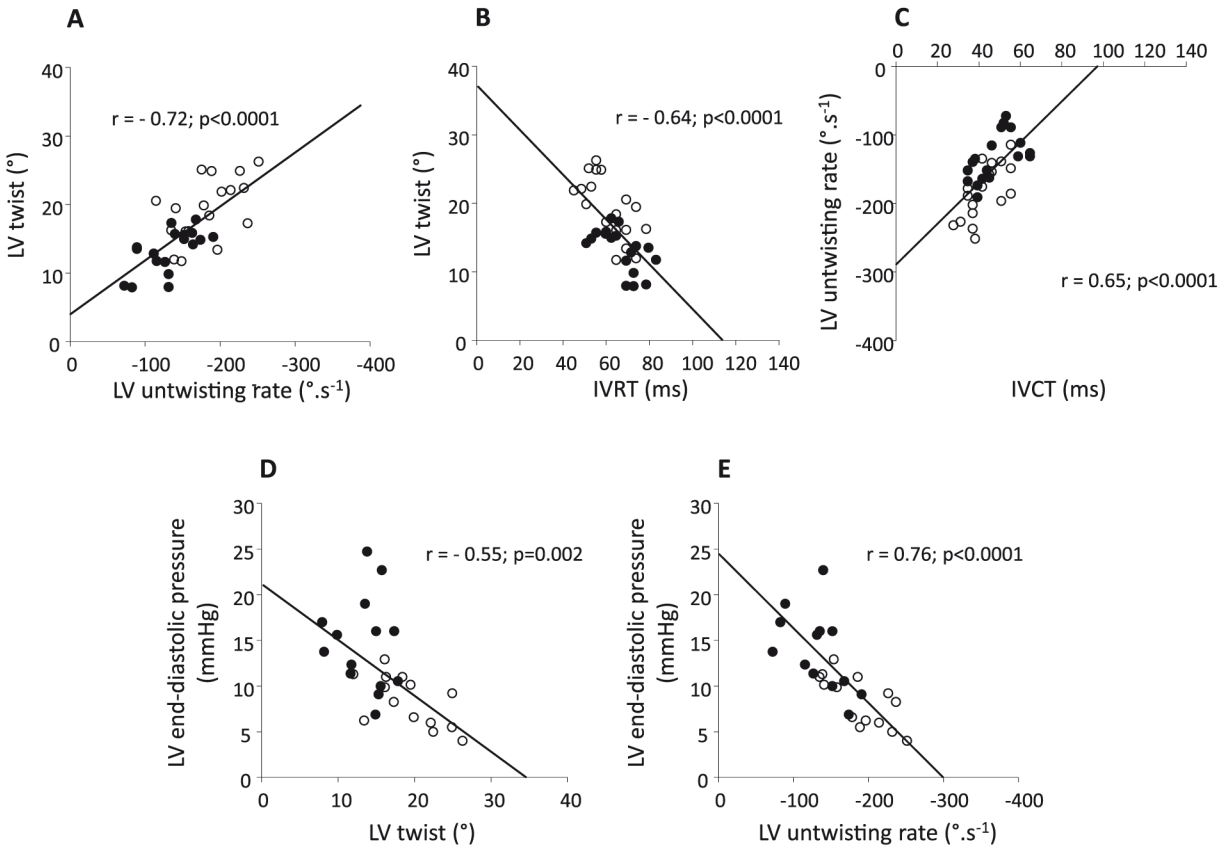

Fig. 2. Contraction-relaxation coupling. Significant linear relationships between left ventricular (LV) twist and untwisting rate (A) (n = 9), LV twist and isovolumic relaxation time (IVRT) (B) (n = 9), LV untwisting rate and isovolumic contraction time (IVCT) (C) (n = 9), LV end-diastolic pressure and LV twist (D) (n = 7) as well as LV end-diastolic pressure and LV untwisting rate (E) (n = 7). Each circle represents individual data obtained at baseline and after dobutamine infusion both at Day 0 (closed circles) and at Day 28 (open circles) after four weeks of angiotensin II infusion.

angiotensin II-infused animals that served as their own control. We previously showed that the occurrence of LV dysfunction and the development of LV hypertrophy is not related to natural growth of these animals. Importantly, all *in vitro* experiments compared samples obtained from saline- *vs* angiotensin II-infused pigs. All these functional alterations in left ventricular function and cardiomyocyte signalling could be the consequences of either direct effect of angiotensin II *per se*, hypertension *per se* induced by angiotensin II or the combination of both.

During systole, the counter-coiled helix of sub-endocardial and sub-epicardial fibers generates rotation of the apex and base of the LV on its longitudinal axis in opposite directions, resulting in LV twist. Measurement of LV twist allows detecting early and subtle LV systolic dysfunction, which is not possible with LV ejection fraction [28,30]. In our experimental conditions, we observed a decrease in LV twist despite unchanged LV ejection fraction. This suggested that pigs developed both sub-endocardial and sub-epicardial dysfunctions rather than sole sub-endocardial dysfunction that would induce unopposed contraction of the sub-epicardial fibers and increase in LV twist [20]. It has been shown that LV twist increases in patients with mild diastolic dysfunction but decreases in those with moderate and severe diastolic dysfunction [21]. Interestingly, in angiotensin II-treated animals, LV end-diastolic pressure was concomitantly increased and was strongly correlated with LV twist impairment, suggesting the contribution of LV twist impairment to LV diastolic dysfunction, in agreement with previous animal [3] and human [22] studies showing that LV twist was a key determinant of LV diastolic suction. Concomitantly, LV untwisting rate was decreased [1,27] and its peak was also delayed in the cardiac cycle after 28 days of angiotensin II infusion, in agreement with previous studies in patients with chronic hypertension and diastolic dysfunction [4,27]. The impairment in LV untwist was also concomitant and correlated with increased LV end-diastolic pressure [22,23]. More importantly, we found that contraction-relaxation remained preserved despite the development of LV hypertrophy and LV dysfunction. This shows that in our experimental conditions, LV diastolic and systolic dysfunctions are necessary concomitant. In such context of tight coupling between contraction and relaxation, it appears that diastolic dysfunction does not occur without systolic alterations. The impact of increase heart in these modifications should also be discussed. There is a clear heart rate-dependency of parameters describing left ventricular function. For example, in normal physiological conditions, there is a clear reduction in isovolumic contraction and relaxation times along with any increase in heart rate [24] and left ventricular filling needs to increase. In this experimental model, the increase in heart rate reveals alterations in left ventricular systolic and diastolic function and particularly, it underlines maladaptive responses to tachycardia that would not be detected in the absence of change in heart rate [12,24,25].

At the cellular level, we observed altered cardiomyocyte shortening and lengthening but the shortening over lengthening rate ratios were not significantly different between saline- and angiotensin II-treated animals highlighting the preserved contraction-relaxation at the cellular level. This supports the cardiomyocyte to play a key role in this contraction-relaxation coupling and its preservation during chronic hypertension and LV hypertrophy. Analysis of calcium transients revealed a significant reduction in Ca^{2+} transient amplitude but diastolic Ca^{2+} and SR Ca^{2+} uptake were not significantly altered in angiotensin II- *vs* saline-treated pigs. Searching for a mechanism of this coupling, we observed abnormal RyR2 channels. Indeed, RyR2 were leaky and we further observed that the RyR2 macromolecular complex was PKA hyperphosphorylated and depleted of its stabilizing protein calstabin2 in

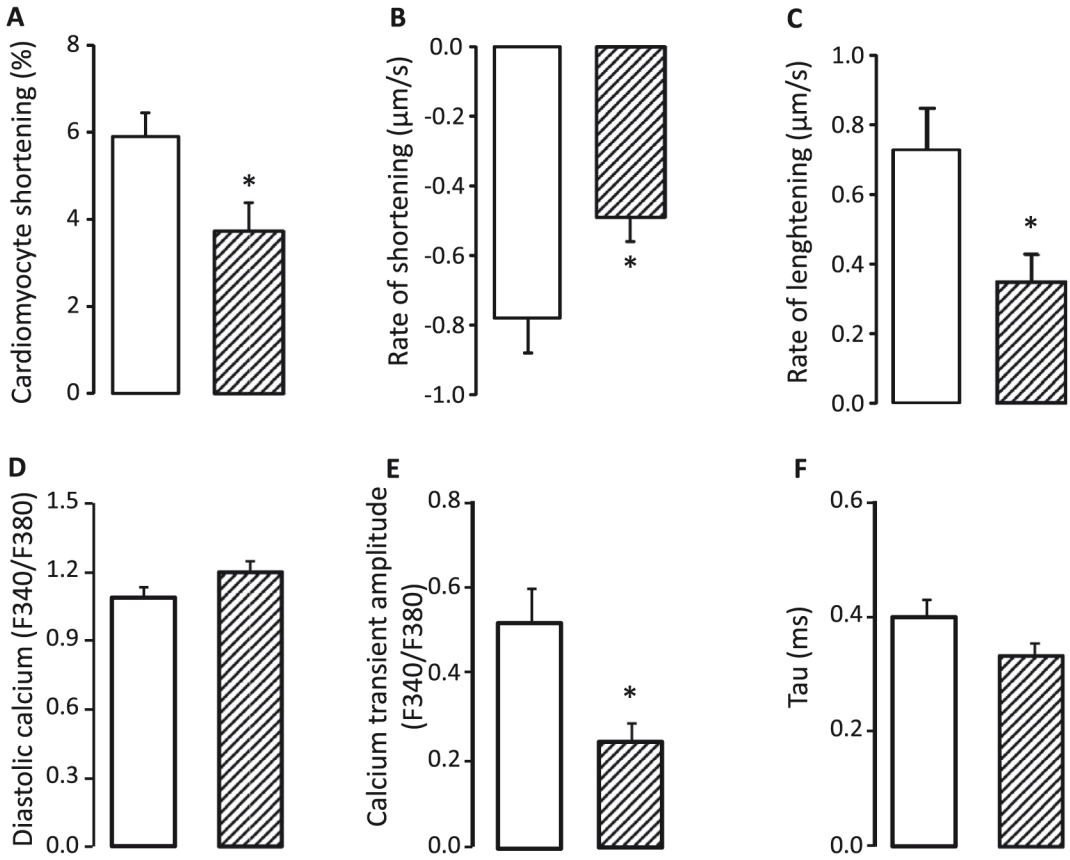

Fig. 3. Altered cardiomyocyte function. Mean ± SEM values of cardiomyocyte shortening (A), rate of shortening (B) and rate of lengthening (C), diastolic calcium (D), calcium amplitude (E) and Tau (F) in cardiomyocytes isolated from saline (n = 9 ABC and 7 DEF, open bars) and angiotensin-II treated (n = 7 ABC and 4 DEF, hatched bars) animals. *p < .05 *vs.* saline.

the angiotensin II-treated pigs. Of note, there was no difference in the oxidation and S-nitrosylation level of RyR2 between saline- and angiotensin II-treated pigs. This remodeling of RyR2 macromolecular complex induces stochastic RyR2 and uncoupled multiple RyR2 channels that may contribute for slower contraction and relaxation [16]. In parallel, expressions of SERCA2a and its regulator PLB were reduced but phosphorylation of phospholamban was concomitantly increased. This suggests that the reduced expression of SERCA appears to be compensated by the higher SERCA activity, although not directly assessed, due to phospho-phospholamban [13] and the reduced amount of calcium released. To our knowledge, the present study is the first to describe such alteration in intracellular Ca^{2+} handling *via* leaky and remodeled RyR2 in the context of LV twist-untwist abnormalities during chronic hypertension and LV hypertrophy. Altered calcium handling with RyR2 and its hyperphosphorylation through calcium leak could participate both to the reduced *in vitro* contraction and thus *in vivo* twist, as well as to slowed *in vitro* relaxation and thus *in vivo* untwist through calcium leak. In the absence of a modification of SR calcium uptake, one can thus hypothesize that part of the leak is temporarily buffered sarcomeric proteins resulting in slower relaxation. This would support RyR2 and its hyperphosphorylation acting on both systole and diastole, *i.e.*, as an integrator of contraction-relaxation coupling. Unfortunately, we could not perform rescue experiments due to the difficulty of having drugs such as RyCal® compounds that could be easily used in pigs to restore normal RyR2 function and subsequent Ca^{2+} handling. Nevertheless, we strongly believe that SR Ca^{2+} leak through RyR2 due to RyR2 hypersensitivity to cytosolic Ca^{2+} and PKA hyperphosphorylation as well as calstabin2 dissociation could represent a common mechanism accounting for both contraction and relaxation alterations. These phenomena could alter systolic Ca^{2+} and impede contraction on the one hand, while on the other hand, leaked RyR2 and impaired expression of SERCA2a and PLB may cause an elevation in diastolic Ca^{2+} affecting the relaxation. Therefore, it is reasonable to hypothesize that as an integrator, RyR2 channels link contraction (systole) and relaxation (diastole). RyR2 alteration would explain preserved contraction-relaxation coupling because aberrant calcium handling occurred simultaneously in both systolic and diastolic periods. Therefore, one may speculate that future therapeutics targeting RyR2 would improve concomitantly LV systolic and diastolic functions in such pathophysiological situation.

Our study has some limitations. We did not precisely investigate the origin of post-translational modifications affecting calcium handling. Increased heart rate indicating a sympathetic activation and Ser 2808 phosphorylation of RyR2 argue for a PKA-dependent mechanism but other players such as CamKII might also be implicated. These functional impairments could also be due to alterations of contractile proteins such as myosin, titin or troponin and other actors involved in the control of calcium homeostasis such as phosphorylated phospholamban. The impact of alterations in cardiac structure should also be discussed. We did not assess fibrosis in the present study, but we previously reported using the same model that angiotensin-II treated animals clearly showed interstitial fibrosis which may have also contributed to the impaired left diastolic function besides abnormal calcium handling. It should be also acknowledged that these animals exhibit rather severe left ventricular hypertrophy.

5. Conclusions

LV contraction-relaxation coupling remained preserved despite LV systolic and diastolic dysfunctions in the present model of chronic

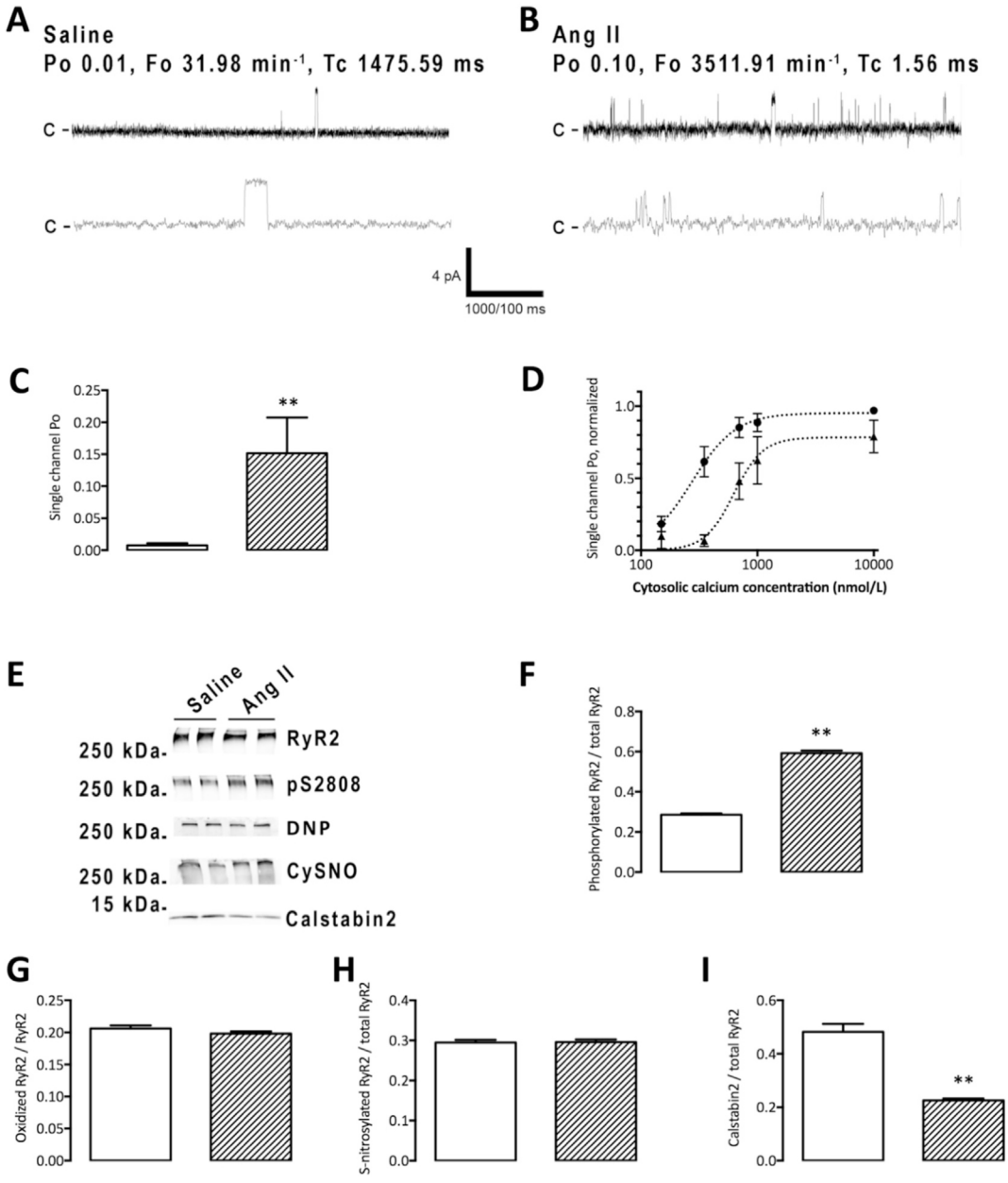

Fig. 4. Leaky ryanodine receptors and post-translational modifications. Representative RyR2 single channel current traces from saline- and angiotensin II-treated (angio II-treated) samples measured at 150 nM [Ca^{2+}] (A and B, respectively). Channel openings are shown as upward deflections; the closed (c -) state is indicated by horizontal bars. Example of channel activity is shown at 5 s (upper trace) and 500 ms (lower trace). (C) Bar graph summarizing single channel Po. n = 11 independent channels for saline and n = 11 for angiotensin II-treated animals. For each condition, the channels were obtained from 3 to 4 animals. (D) RyR2 normalized Po from 150 nmol/L to 10 μmol/L. Each data point represents the Po calculated as an average from 4 to 13 independent channels obtained from 3 to 4 animals. RyR2 Ca^{2+} dependences were fitted by a one-site binding (Hill slope) equation. Data presented as mean ± SEM. *p < .05 *vs.* saline, **p < .01 *vs.* saline. (E) Representative immunoblots of saline-treated (saline) and angiotensin II-treated (Ang II) samples. RyR2 were immunoprecipitated from tissue lysate using an anti-RyR2 antibody. Bands of total RyR2, PKA-phosphorylated RyR2 at S2808 site, DNP (oxidized RyR2), CysNO (S-nitrosylated RyR2) and Calstabin2 binding are shown. (F–I) Normalization of data from immunoblots for the relative RyR2 PKA phosphorylation, oxidation, S-nitrosylation and calstabin2 bound to RyR2 macromolecular complex in saline- (open bars) and angiotensin II- (hatched bars) treated animals. Data are presented as mean ± SEM. n = 8 for saline- and n = 12 for angiotensin II-treated animals. For each condition, the number of experiments is related to independent blots obtained from 4 to 5 animals. **p < .01 *vs.* saline.

hypertension and LV hypertrophy. This *in vivo* disturbance occurs through an impairment of cardiac contraction and relaxation. At the cellular level, SR Ca^{2+} leak through PKA hyperphosphorylated RyR2, depleted of its stabilizing calstabin2 partner may contribute to both contraction and relaxation alterations. These results suggest that RyR2, as an integrator, may contributes to control LV contraction-relaxation coupling. LV diastolic dysfunction was accompanied by LV systolic dysfunction, *i.e.*, the discovery of LV diastolic dysfunction with preserved ejection fraction in patients should imply the track of LV systolic dysfunction.

Sources of funding

This work was supported by grants from the “Société Française d'Hypertension Artérielle” (2010), the “Fondation de l'Avenir” (ET9-529, ET2-648), the “Association Française contre les Myopathies” (AFM; project 16073, MNM2 2012), the “Fondation de la Recherche Médicale” (FRM; SPF20130526710). This work was also supported by

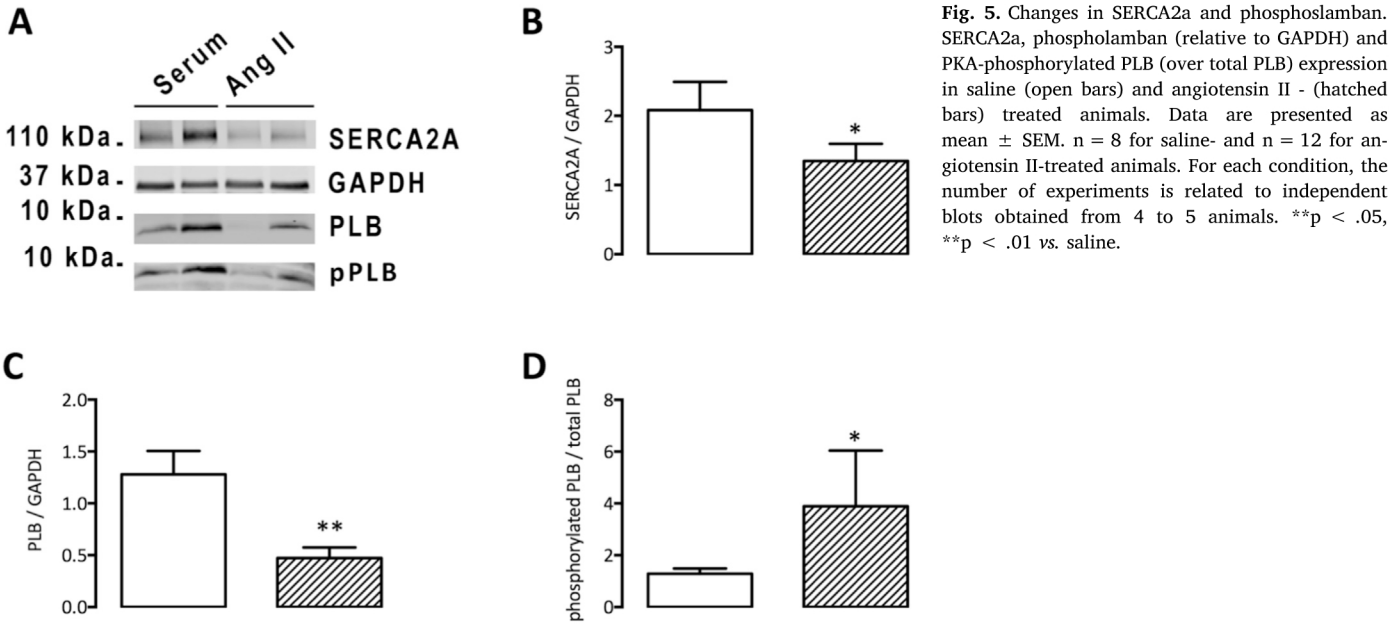

Fig. 5. Changes in SERCA2a and phosphoslamban. SERCA2a, phospholamban (relative to GAPDH) and PKA-phosphorylated PLB (over total PLB) expression in saline (open bars) and angiotensin II - (hatched bars) treated animals. Data are presented as mean ± SEM. n = 8 for saline- and n = 12 for angiotensin II-treated animals. For each condition, the number of experiments is related to independent blots obtained from 4 to 5 animals. **p < .05, **p < .01 *vs.* saline.

grants from the “Institut National pour la Santé et la Recherche Médicale” (INSERM), the “Région Ile de France” (CODDIM), the “Université Paris Est Créteil” (UPEC) and the “Ecole Nationale Vétérinaire d'Alfort” (ENVA).

Disclosures

None.

References

[1] M.I. Ahmed, R.V. Desai, K.K. Gaddam, B.A. Venkatesh, S. Agarwal, S. Inusah, S.G. Lloyd, T.S. Denney Jr., D. Calhoun, L.J. Dell'italia, H. Gupta, Relation of torsion and myocardial strains to LV ejection fraction in hypertension, JACC Cardiovasc. Imaging 5 (2012) 273–281, https://doi.org/10.1016/j.jcmg.2011.11.013.

[2] C.C. Beladan, A. Calin, M. Rosca, C. Ginghina, B.A. Popescu, Left ventricular twist dynamics: principles and applications, Heart 100 (2013) 731–740 (doi:heartjnl-2012-302064 [pii]10.1136/heartjnl-2012-302064).

[3] S.P. Bell, L. Nyland, M.D. Tischler, M. McNabb, H. Granzier, M.M. LeWinter, Alterations in the determinants of diastolic suction during pacing tachycardia, Circ. Res. 87 (2000) 235–240.

[4] A.T. Burns, A. La Gerche, D.L. Prior, A.I. Macisaac, Left ventricular untwisting is an important determinant of early diastolic function, JACC Cardiovasc. Imaging 2 (2009) 709–716 (doi:S1936-878X(09)00206-X [pii]10.1016/j.jcmg.2009.01.015).

[5] V. Celic, M. Tadic, J. Suzic-Lazic, A. Andric, A. Majstorovic, B. Ivanovic, P. Stevanovic, O. Iracek, R. Scepanovic, Two- and three-dimensional speckle tracking analysis of the relation between myocardial deformation and functional capacity in patients with systemic hypertension, Am. J. Cardiol. 113 (2014) 832–839, https://doi.org/10.1016/j.amjcard.2013.11.031.

[6] J.W. Cheung, A.C. Meli, W. Xie, S. Mittal, S. Reiken, A. Wronska, L. Xu, J.S. Steinberg, S.M. Markowitz, S. Iwai, A. Lacampagne, B.B. Lerman, A.R. Marks, Short-coupled polymorphic ventricular tachycardia at rest linked to a novel ryanodine receptor (RyR2) mutation: leaky RyR2 channels under non-stress conditions, Int. J. Cardiol. 180 (2015) 228–236, https://doi.org/10.1016/j.ijcard.2014.11.119.

[7] G. Doucende, I. Schuster, T. Rupp, A. Startun, M. Dauzat, P. Obert, S. Nottin, Kinetics of left ventricular strains and torsion during incremental exercise in healthy subjects: the key role of torsional mechanics for systolic-diastolic coupling, Circ. Cardiovasc. Imaging 3 (2010) 586–594, https://doi.org/10.1161/CIRCIMAGING.110.943522.

[8] J. Fauconnier, J.L. Pasquie, P. Bideaux, A. Lacampagne, S. Richard, Cardiomyocytes hypertrophic status after myocardial infarction determines distinct types of arrhythmia: role of the ryanodine receptor, Prog. Biophys. Mol. Biol. 103 (2010) 71–80, https://doi.org/10.1016/j.pbiomolbio.2010.01.002.

[9] J. Fauconnier, J. Thireau, S. Reiken, C. Cassan, S. Richard, S. Matecki, A.R. Marks, A. Lacampagne, Leaky RyR2 trigger ventricular arrhythmias in Duchenne muscular dystrophy, Proc. Natl. Acad. Sci. U. S. A. 107 (2010) 1559–1564, https://doi.org/10.1073/pnas.0908540107.

[10] M.S. Firstenberg, N.G. Smedira, N.L. Greenberg, D.L. Prior, P.M. McCarthy, M.J. Garcia, J.D. Thomas, Relationship between early diastolic intraventricular pressure gradients, an index of elastic recoil, and improvements in systolic and diastolic function, Circulation 104 (2001) I330–I335, https://doi.org/10.1161/hc37t1.094834.

[11] S.A. Goonasekera, K. Hammer, M. Auger-Messier, I. Bodi, X. Chen, H. Zhang, S. Reiken, J.W. Elrod, R.N. Correll, A.J. York, M.A. Sargent, F. Hofmann, S. Moosmang, A.R. Marks, S.R. Houser, D.M. Bers, J.D. Molkentin, Decreased cardiac L-type Ca(2)(+) channel activity induces hypertrophy and heart failure in mice, J. Clin. Invest. 122 (2012) 280–290, https://doi.org/10.1172/JCI58227.

[12] M. Jozwiak, J. Melka, M. Rienzo, A. Bize, L. Sambin, L. Hittinger, A. Berdeaux, J.B. Su, B. Bouhemad, B. Ghaleb, Ivabradine improves left ventricular twist and untwist during chronic hypertension, Int. J. Cardiol. 252 (2018) 175–180, https://doi.org/10.1016/j.ijcard.2017.11.049.

[13] E.G. Kranias, R.J. Hajjar, Modulation of cardiac contractility by the phopholamban/SERCA2a regulatome, Circ. Res. 110 (2012) 1646–1660, https://doi.org/10.1161/CIRCRESAHA.111.259754.

[14] R.M. Lang, M. Bierig, R.B. Devereux, F.A. Flachskampf, E. Foster, P.A. Pellikka, M.H. Picard, M.J. Roman, J. Seward, J.S. Shanewise, S.D. Solomon, K.T. Spencer, M.S. Sutton, W.J. Stewart, Recommendations for chamber quantification: a report from the American Society of Echocardiography's Guidelines and Standards Committee and the Chamber Quantification Writing Group, developed in conjunction with the European Association of Echocardiography, a branch of the European Society of Cardiology, J. Am. Soc. Echocardiogr. 18 (2005) 1440–1463 (doi:S0894-7317(05)00983-1 [pii]10.1016/j.echo.2005.10.005).

[15] N. Maharaj, B.K. Khandheria, F. Peters, E. Libhaber, M.R. Essop, Time to twist: marker of systolic dysfunction in Africans with hypertension, Eur. Heart J. Cardiovasc. Imaging 14 (2013) 358–365, https://doi.org/10.1093/ehjci/jes175.

[16] S.O. Marx, J. Gaburjakova, M. Gaburjakova, C. Henrikson, K. Ondrias, A.R. Marks, Coupled gating between cardiac calcium release channels (ryanodine receptors), Circ. Res. 88 (2001) 1151–1158, https://doi.org/10.1161/hh1101.091268.

[17] A.C. Meli, M.M. Refaat, M. Dura, S. Reiken, A. Wronska, J. Wojciak, J. Carroll, M.M. Scheinman, A.R. Marks, A novel ryanodine receptor mutation linked to sudden death increases sensitivity to cytosolic calcium, Circ. Res. 109 (2011) 281–290, https://doi.org/10.1161/CIRCRESAHA.111.244970.

[18] Y. Mizuguchi, Y. Oishi, H. Miyoshi, A. Iuchi, N. Nagase, T. Oki, Concentric left ventricular hypertrophy brings deterioration of systolic longitudinal, circumferential, and radial myocardial deformation in hypertensive patients with preserved left ventricular pump function, J. Cardiol. 55 (2010) 23–33, https://doi.org/10.1016/j.jjcc.2009.07.006.

[19] S.F. Nagueh, C.P. Appleton, T.C. Gillebert, P.N. Marino, J.K. Oh, O.A. Smiseth, A.D. Waggoner, F.A. Flachskampf, P.A. Pellikka, A. Evangelisa, Recommendations for the evaluation of left ventricular diastolic function by echocardiography, Eur. J. Echocardiogr. 10 (2009) 165–193 (doi:jep007 [pii]10.1093/ejechocard/jep007).

[20] A.M. Omar, S. Vallabhajosyula, P.P. Sengupta, Left ventricular twist and torsion: research observations and clinical applications, Circ. Cardiovasc. Imaging 8 (2015), https://doi.org/10.1161/CIRCIMAGING.115.003029.

[21] S.J. Park, C. Miyazaki, C.J. Bruce, S. Ommen, F.A. Miller, J.K. Oh, Left ventricular torsion by two-dimensional speckle tracking echocardiography in patients with diastolic dysfunction and normal ejection fraction, J. Am. Soc. Echocardiogr. 21 (2008) 1129–1137 (doi:S0894-7317(08)00195-8 [pii]10.1016/j.echo.2008.04.002).

[22] S.J. Park, R.A. Nishimura, B.A. Borlaug, P. Sorajja, J.K. Oh, The effect of loading alterations on left ventricular torsion: a simultaneous catheterization and two-dimensional speckle tracking echocardiographic study, Eur. J. Echocardiogr. 11 (2010) 770–777, https://doi.org/10.1093/ejechocard/jeq064.

[23] R. Perry, C.G. De Pasquale, D.P. Chew, M.X. Joseph, Assessment of early diastolic left ventricular function by two-dimensional echocardiographic speckle tracking,

Eur. J. Echocardiogr. 9 (2008) 791–795, https://doi.org/10.1093/ejechocard/jen148.
[24] M. Rienzo, A. Bize, D. Pongas, S. Michineau, J. Melka, H.L. Chan, L. Sambin, J.B. Su, J.L. Dubois-Rande, L. Hittinger, A. Berdeaux, B. Ghaleh, Impaired left ventricular function in the presence of preserved ejection in chronic hypertensive conscious pigs, Basic Res. Cardiol. 107 (2012) 298, , https://doi.org/10.1007/s00395-012-0298-9.
[25] M. Rienzo, J. Melka, A. Bize, L. Sambin, M. Jozwiak, J.B. Su, L. Hittinger, A. Berdeaux, B. Ghaleh, Ivabradine improves left ventricular function during chronic hypertension in conscious pigs, Hypertension 65 (2015) 122–129, https://doi.org/10.1161/HYPERTENSIONAHA.114.04323.
[26] J. Shan, M.J. Betzenhauser, A. Kushnir, S. Reiken, A.C. Meli, A. Wronska, M. Dura, B.X. Chen, A.R. Marks, Role of chronic ryanodine receptor phosphorylation in heart failure and beta-adrenergic receptor blockade in mice, J. Clin. Invest. 120 (2010) 4375–4387, https://doi.org/10.1172/JCI37649.
[27] M. Takeuchi, W.B. Borden, H. Nakai, T. Nishikage, M. Kokumai, T. Nagakura, S. Otani, R.M. Lang, Reduced and delayed untwisting of the left ventricle in patients with hypertension and left ventricular hypertrophy: a study using two-dimensional speckle tracking imaging, Eur. Heart J. 28 (2007) 2756–2762 (doi:ehm440 [pii] 10.1093/eurheartj/ehm440).
[28] Y.T. Tan, F. Wenzelburger, E. Lee, G. Heatlie, F. Leyva, K. Patel, M. Frenneaux, J.E. Sanderson, The pathophysiology of heart failure with normal ejection fraction: exercise echocardiography reveals complex abnormalities of both systolic and diastolic ventricular function involving torsion, untwist, and longitudinal motion, J. Am. Coll. Cardiol. 54 (2009) 36–46 (doi:S0735-1097(09)01169-3 [pii]10.1016/j.jacc.2009.03.037).
[29] G.J. Wang, L.Y. Guo, H.X. Wang, Y.S. Yao, IP3R and RyR calcium channels are involved in neonatal rat cardiac myocyte hypertrophy induced by tumor necrosis factor-alpha, Am. J. Transl. Res. 9 (2017) 343–354.
[30] G.W. Yip, Q. Zhang, J.M. Xie, Y.J. Liang, Y.M. Liu, B. Yan, Y.Y. Lam, C.M. Yu, Resting global and regional left ventricular contractility in patients with heart failure and normal ejection fraction: insights from speckle-tracking echocardiography, Heart 97 (2011) 287–294 (doi:hrt.2010.205815).